

# Critical Solutions of Three Vortex Motion in the Parabolic Case

L. Ting

New York University, Courant Institute of Mathematical Sciences

New York, NY 10012, USA

O. Knio

The Johns Hopkins University, Department of Mechanical Engineering

Baltimore, MD 21218, USA

D. Blackmore

New Jersey Institute of Technology, Department of Mathematical Sciences

Newark, NJ 07102, USA

November 16, 2018

## Abstract

Gröbli (1877) laid the foundation for the analysis of the motion of three point vortices in a plane by deriving governing equations for triangular configuration of the vortices. Synge (1949) took this formulation one step further to that of a similar triangle of unit perimeter, via trilinear coordinates. The final reduced problem is governed by an integrable two-dimensional system of differential equations with solutions represented as planar trajectories. Another key to Synge's analysis was his classification of the problem into three distinct cases: elliptic, hyperbolic and parabolic corresponding, respectively, to the sum of products

---

<sup>0</sup>Correspondence, *E-mail address*: ting@cims.nyu.edu

of pairs of vortex strengths being positive, negative or zero. The reduction of the vortex configuration, a curve in space to a planar curve is one-to-one, except along a critical planar curve  $\mathcal{C}$  in the parabolic case. Each point on  $\mathcal{C}$  represents a triangle of unit perimeter corresponding to a family of similar vortex configurations, expanding or contracting. The latter would lead to coalescence of the three vortices. Tavantzis and Ting (1988) filled most of the gaps left by Synge regarding the dynamics of the problem, and showed in particular that points on  $\mathcal{C}$  corresponding to similar expanding families of vortex configurations are stable while those corresponding to similar contracting families are unstable. Their investigations yielded an exhaustive description of the motion and stability of three vortices in a plane except for the global behavior of the vortex configurations in a narrow strip containing  $\mathcal{C}$ . The main contribution of this paper is a complete description of the global dynamics in such a strip, which emphatically demonstrates that three distinct vortices almost never coalesce.

*Keywords:* Three point vortices; Trilinear coordinates, Parabolic case; Critical curve.

## 1 Introduction

The planar motion of three point vortices in an incompressible fluid was studied by Gröbli in 1877 [1] and Synge in 1949 [2] among others. With the aid of the integral invariants, Gröbli uncoupled the autonomous six-degree of freedom problem to the study the vortex configuration and the translation and rotation of the configuration and essentially demonstrated the integrability of the system. The vortex configuration problem refers to the deformations of the triangle,  $\Delta_p(t)$ , formed by the three point vortices at  $z_j(t)$  in the complex  $z$ -plane. The triangle is defined by the lengths,  $R_j(t)$ ,  $j = 1, 2, 3$ , of its sides, with the  $j$ -th side facing the  $j$ -th vortex. The subscript  $p$  denotes the perimeter,  $p = R_1 + R_2 + R_3$ , shown in Fig. 1 (a). It is a three degree of freedom problem and is integrable, with the integral curves, or spatial

trajectories,  $\mathbf{R}(t)$ , in Cartesian coordinates,  $R_j(t)$ , given by Synge [2]. The solution was further simplified by Synge [2] who introduced the trilinear coordinates  $x_j$ ,  $j = 1, 2, 3$  with  $x_j = R_j/p$ . As shown in Fig. 1 (b), the spatial integral curve,  $\mathbf{R}(t)$  is projected radially onto the plane,  $\mathcal{P}$ , which intersects the  $j$ -th axis at  $P_j$  with intercept  $\sqrt{2/3}$ . Its cross-section in the first octant is the equilateral  $\triangle P_1P_2P_3$  with side  $2/\sqrt{3}$  and height 1, as shown in Fig. 1 (b). The heavy dot on the plane  $\mathcal{P}$  with position vector  $\sqrt{2/3}\mathbf{R}/p$ , denotes the radial projection of  $\mathbf{R}$ . The trilinear coordinates,  $x_j$ 's, in turn denote the distances from the heavy dot to the sides of the triangle  $P_1P_2P_3$  opposite to the vertices  $P_j$ 's, as shown by the thin lines. Note that the sum,  $x_1 + x_2 + x_3 = 1$ , is the height of the triangle  $P_1P_2P_3$ . The trilinear coordinates represent the sides of  $\triangle_1(t)$  with perimeter 1, which is similar to and has the same orientation as  $\triangle_p$  in Fig. 1 (a).

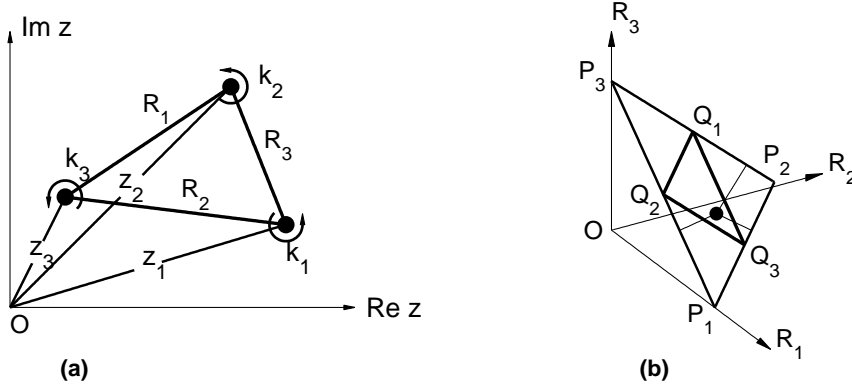


Figure 1: (a) The triangle  $\triangle_p$  formed by the three point vortices at  $z_j(t)$ ,  $j = 1, 2, 3$ , in the complex  $z$ -plane, and (b) the coordinate axes,  $R_1, R_2$  and  $R_3$ , the plane  $\mathcal{P}$  or the  $\alpha\beta$  plane and the trilinear coordinates  $x_j$ , shown as the lines from a point, the heavy dot, on  $\mathcal{P}$  to its edges in the first octant.

Because of the triangle inequality, the admissible solutions,  $x_j$  of  $\triangle_1$ , are confined to  $\triangle Q_1Q_2Q_3$  and a point on its positive (negative) side with normal vector pointing away from

(towards) the origin  $O$  corresponds to a configuration  $\Delta_p$  with the three vortices in counter-clockwise (clockwise) orientation. Two points on the opposite sides of  $\mathcal{P}$  with the same  $x_j$  are called the image points of each other.

Synge [2] identified the sum of the products of the vortex strengths,  $k_j$ ,

$$K = k_1 k_2 + k_2 k_3 + k_3 k_1, \quad (1)$$

as the primary parameter, and described the topologies of the integral curves and critical points in the plane  $\mathcal{P}$  according to the classifications,

$$\text{elliptic; } K > 0; \quad \text{parabolic; } K = 0; \quad \text{and} \quad \text{hyperbolic, } K < 0. \quad (2)$$

In particular, he studied the critical point,  $\mathbf{E}$ , at the centroid of  $\Delta P_1 P_2 P_3$  and also that of  $\Delta Q_1 Q_2 Q_3$  ( $\Delta_Q$  for short hereafter) on the positive side of  $\mathcal{P}$ , where  $x_j = 1/3$ . The corresponding configuration is an equilateral triangle and was shown to be stable (unstable) for the elliptical (hyperbolic) cases. This is true also for the image of  $E$ , the centroid  $E^*$  on the negative side of  $\mathcal{P}$ .

For the parabolic case, Synge pointed out that the critical point  $E$  lies on a critical curve  $\mathcal{C}$  and partitions  $\mathcal{C}$  into expanding and contracting branches, while the images of those two branches on  $\mathcal{C}^*$  are contracting and expanding, respectively. The study of the local stability and global trajectories near these two branches on  $\mathcal{C}$  and their images is the main subject of this paper.

The planar vortex problem was studied via Hamiltonian formalism by Lin in 1943, [10], Novikov in 1975 [3], Aref in 1979 [4] among others. Tavantzis and Ting in 1988 [5] continued Synge's analysis via trilinear coordinates. For each classification by  $K$  in (2), they located all the critical points and studied their stability and described the topologies of the integral curves and separatrices in the plane  $\mathcal{P}$ .

Numerical studies of the motions of three vortices in a half-plane were carried out by Knio et al. [6]. for vortices of equal strength,  $k$ , i. e.,  $K = 3k^2 > 0$  in the elliptic cases. The numerical results showed that the motion of the vortices can be regular or chaotic depending on their initial configuration, which was taken to be either an equilateral triangle or collinear. The transition from regular to chaotic for those half plane problems can be anticipated when the distances between the vortices are much smaller than their distances from the boundary. The half plane problems can then be considered as perturbations of three vortices in the entire plane, for which the equilateral configuration corresponds to a center while the collinear configuration corresponds to a saddle point in elliptic cases, [2]. This observation motivated a sequence of theoretical and numerical studies of perturbed three vortex problems in parallel with the classical perturbed two body problems. Here the perturbations arise for example from the presence of a boundary and/or additional vortices far away from the three main vortices or from the approximations the interactions of three coaxial vortex rings by three vortices in a meridian plane when the distances between the rings are much smaller than the radii of the rings. See the article by Blackmore et al. [7] and the references therein and recent studies by Ting et al. [8] and Knio et al. [9]. Several numerical examples were presented to show transitions from periodic and quasi-periodic to chaotic regimes in accordance with the theoretical results.

This paper does not deal with perturbations. Rather, it presents an exhaustive study of the global behavior of the dynamics of three vortices in a plane in parabolic cases, with initial vortex configurations in a narrow strip containing the critical curve  $\mathcal{C}$ . This completes the local stability analysis of  $\mathcal{C}$  presented Tavantzis and Ting [5].

For the strengths of three vortices, at least two of them have to have the same sign. Thus we can always choose the sign of those two to be positive and denote them by  $k_1$  and  $k_2$  with

$$k_1 \geq k_2 > 0, \quad \text{and} \quad k_3 = -k_1 k_2 / (k_1 + k_2) < 0, \quad (3)$$

for the parabolic case,  $K = 0$ . After ordering the three vortices by Eq. (3), the initial positions of the vortices  $z_j(0)$  in the  $z$ -plane define the sides  $R_j(0)$  of the triangle  $\Delta_p$  and hence the trilinear coordinates  $x(0)$  in the plane  $\mathcal{P}$  and in addition the orientations of the vortex configuration, clockwise or counterclockwise, denoted by the index  $\gamma = +1$  and  $-1$ , respectively. To account for the opposite orientations,  $\gamma = \pm 1$ , Synge made use of both sides, the positive and negative sides, of  $\mathcal{P}$ , or  $\Delta P_1 P_2 P_3$ . The normal vector to the positive or the negative side, points away from or towards the origin  $O$ , respectively, (see Fig. 1). He assigned the points  $x_j$  with  $\gamma = +1$  ( $\gamma = -1$ ) to be on the positive (negative) side of  $\Delta P_1 P_2 P_3$ . A change of orientation can take place only when crossing over an edge of the triangle.

It was pointed out by Synge [2] that the mapping from a point  $\mathbf{R}$  on the spatial integral curve to its radial projection onto a point on the planar curve in  $\mathcal{P}$ , is one to one if the velocity  $\dot{\mathbf{R}}(t)$  is not in the radial direction, i. e.,  $\dot{\mathbf{R}} \times \mathbf{R} \neq 0$ , which can occur only on a planar critical curve  $\mathcal{C}$  in a parabolic case. The critical curve is partitioned into expanding and contracting branches. Corresponding to a point on the curve,  $\mathcal{C}$ , the sides  $x_j$ 's of the  $\Delta_1$  remain stationary, while  $\Delta_p(t)$ , similar to  $\Delta_1$ , is expanding, with  $\dot{p} > 0$  on one branch and contracting  $\dot{p} < 0$  on the adjacent branch. It was shown in [5] that the similar expanding solution is stable while the contracting one is unstable. Similar contracting solutions, albeit unstable, have received attention because they could in principle lead to simultaneous colliding or coalescence of three vortices (see for example Newton [11], pp. 84-88). Thus we need to reinforce the local instability analysis of [5], for a point on a contracting branch of  $\mathcal{C}$  by nonlocal analysis leading to the conclusion that coalescence of three vortices is unlikely.

In Sec. 2 we present a brief review of the three point vortex problem, define the symbols, and summarize the relevant results of Synge [2] and Tavantzis and Ting [5]. To render this paper self-contained, we reproduce derivations and descriptions of results relevant to the current

investigation, namely, the spatial trajectories of vortex configurations and their reduction to planar trajectories via trilinear coordinates.

In Sec. 3, we study in detail the planar trajectories and the critical curve  $\mathcal{C}$  in parabolic cases. We extend the local stability analysis of the critical curve in [5] by showing that a small deviation off  $\mathcal{C}$  from a point on a contracting branch produces a trajectory that departs from the neighborhood of  $\mathbf{x}$  and is finally attracted to an expanding branch of the critical curve. Depending on the location of the point  $\mathbf{x}$  on  $\mathcal{C}$  and the perturbation of  $\mathbf{x}$  to a point above or below  $\mathcal{C}$ , we identify three types of trajectories. An outline of this investigation was presented recently by Ting and Blackmore [12].

In Sec. 4 we present numerical examples to demonstrate how the the configuration  $\Delta_1$  departs from the neighborhood of a contracting branch of the critical curve  $\mathcal{C}$  along a trajectory to the expanding branch. We show the three types of trajectories and the variations of the configurations depending on the locations of initial point  $\mathbf{x}$ , as predicted in Sec. 3.

## 2 Background

Adopting the symbols of [2] and [5], we relate the strength of a vortex  $k_j$  to its circulation  $\Gamma_j$  by  $k_j = \Gamma_j/2\pi$ ,  $j = 1, 2, 3$ , and denote the position of the  $j$ -th vortex in the complex plane by  $z_j(t) = \Re z_j + i\Im z_j$ , and the length of the side of  $\Delta_p$  facing its  $j$ -th vertex at  $z_j$  by  $R_j$ .

Without loss of generality, we assign the strengths of the three vortices according to Eq. (3). We set the initial perimeter as the length scale,  $p(0) = 1$  and then the time scale is defined by  $p^2(0)/k_2$ . The equations of motion of three point vortices in a planar incompressible inviscid flow are:

$$\dot{z}_j(t) = -i \sum_{m \neq j} \frac{k_m}{\bar{z}_m - \bar{z}_j}, \quad \text{for } j = 1, 2, 3. \quad (4)$$

The summation in  $m$  ranges over 1, 2, and 3. We obtain from Eq. (4) the well-known theory of

Kirchhoff or the conservation laws of vorticity and the moment of vorticity in the  $z$ -plane ([13], pp. 229-230),

$$\sum_j k_j \dot{z}_j = 0, \quad \text{and} \quad \sum_j k_j \bar{z}_j \dot{z}_j(t) = iK \quad (5)$$

The second equation in polar coordinates yields

$$\sum_j k_j \rho_j^2 = \text{const.} \quad \text{and} \quad \sum_j k_j \rho_j^2 \dot{\theta}_j = K, \quad (6)$$

where  $\rho_j$  and  $\theta_j$  denote the magnitude and argument of  $z_j$ , respectively.

In the next section, we will reproduce the analyses of Gröbli (1877) and Synge (1949) which decoupled the six equations for the real and imaginary parts of Eq. (4),  $j = 1, 2, 3$ , to three equations for  $R_j$ , the vortex configuration and three for the motion of the configuration. The equations for the latter will come from the above two conservation equations in (5).

## 2.1 Deformation of the configuration $\Delta_p$

The deformations of  $R_j$ 's are governed by linear combinations of Eq. (4). For example, from a linear combination of the first two equations (4), we get

$$(\bar{z}_1 - \bar{z}_2)(\dot{z}_1 - \dot{z}_2) = R_3 \dot{R}_3 + iR_3^2 \dot{\psi}_{21} = i(k_1 + k_2) - ik_3 R_3 [R_2^{-1} e^{i[\psi_{13} - \psi_{21}]} - R_1^{-1} e^{i[\psi_{23} - \psi_{21}]}]. \quad (7)$$

Here  $\psi_{jl}$  denotes the argument of the side  $z_l - z_j$ , and  $\psi_{lj} = \psi_{jl} + \pi$  denotes that of  $z_j - z_l$ . The real part of the equation yields the rate of change of the side  $R_3 = |z_1 - z_2|$ . Likewise, Synge [2] obtained the rates of change of all three sides of  $\Delta_p$ ,

$$\frac{\dot{R}_1}{k_1 R_1 (R_3^2 - R_2^2)} = \frac{\dot{R}_2}{k_2 R_2 (R_1^2 - R_3^2)} = \frac{\dot{R}_3}{k_3 R_3 (R_2^2 - R_1^2)} = \frac{2\gamma|A|}{R_1^2 R_2^2 R_3^2}. \quad (8)$$

where  $|A| = [s(s - R_1)(s - R_2)(s - R_3)]^{1/2}$ , with  $s = p/2$ , stands for the area of  $\Delta_p$ . From the initial data for the  $z_j$ 's, we have the data for the  $R_j$ 's of the  $\Delta_l$  and then Eqs. (8) define the spatial integral curve,  $\mathbf{R}(t)$ , in the first octant, where  $R_j > 0$ ,  $j = 1, 2, 3$ . The integral curve  $\mathcal{R}$



is defined directly by the two integral invariants, or by the intersection of two surfaces,

$$k_1^{-1}R_1^2 + k_2^{-1}R_2^2 + k_3^{-1}R_3^2 = \text{initial value } a \quad (9)$$

$$R_1^{1/k_1} R_2^{1/k_2} R_3^{1/k_3} = \text{initial value } b. \quad (10)$$

They were obtained by Kirchhoff for  $N$ -vortices, with  $N = 3$  here, (see e. g. [13, page 230]).

From  $\dot{\mathbf{R}}(t)$ , we define the direction along the integral curve and call the directed integral curve the trajectory of the configuration, or simply the trajectory.

To recover the positions  $z_j(t)$  corresponding to a point on the integral curve  $\mathcal{R}$ , we need to find three combinations of the primary six equations in (4) independent of the three equations for the configuration (8). These three combinations appear readily from the real and imaginary parts of the conservation of the center of vorticity in (5) and the imaginary part of the polar moment of vorticity in Eqs. (6). The real part of the equation for the polar moment is not independent because it is equivalent to Eq. (9), see [2].

We first find the dependence of  $R_j$  and their inclinations, say  $R_3$  and  $\psi_{12}$ , on  $t$  by integrating Eq. (8). That would then define the temporal variations of the configuration  $\Delta_p$  and its inclination. Finally the locations  $z_j(t)$  of the vertices of  $\Delta_p(t)$  are defined by the first invariant in (5), or by locating the (stationary) weighted center of  $\Delta_p(t)$ ,  $z_c = (k_1 z_1(0) + k_2 z_2(0) + k_3 z_3(0))/(k_1 + k_2 + k_3)$ , for  $k_1 + k_2 + k_3 \neq 0$ , which holds for parabolic cases.

The reduction of the spatial curve  $\mathbf{R}$  to a planar curve by Synge [2] via trilinear coordinates is outlined in the next subsection.

## 2.2 The trilinear coordinates

Synge [2] projected the point  $\mathbf{R}$  radially onto the point,  $\mathbf{q}$  on the plane  $\mathcal{P}$ ,

$$R_1 + R_2 + R_3 = \sqrt{2/3}, \quad (11)$$

which intersects the axes respectively at  $P_1$ ,  $P_2$  and  $P_3$ , with equal intercept,  $\sqrt{2/3}$ . The plane  $\mathcal{P}$  intersects the coordinate planes at the same angle,  $\arcsin \sqrt{2/3}$ . As shown in Fig. 1 (b), the equilateral  $\triangle P_1 P_2 P_3$  denotes the section of  $\mathcal{P}$  in the first octant with each side  $2/\sqrt{3}$  and height  $H = 1$ . The trilinear coordinates  $x_j$ ,  $j = 1, 2, 3$  of point  $\mathbf{q}$  in  $\mathcal{P}$  are the signed distances from the sides of  $\triangle P_1 P_2 P_3$ . The sign of the distance from a side is positive (negative) if the distance from the side to  $\mathbf{q}$  points inwards to (outward from)  $\triangle P_1 P_2 P_3$ . The sum of the trilinear coordinates is always equal to the height  $H$ ,

$$x_1 + x_2 + x_3 = 1. \quad (12)$$

The  $x_j$ 's are all positive when  $\mathbf{q}$  lies inside  $\triangle P_1 P_2 P_3$  and are related to the Cartesian coordinates  $R'_j$  of  $\mathbf{q}$  by,

$$\frac{R'_j}{x_j} = \sqrt{\frac{2}{3}}, \quad \text{while} \quad \frac{R_j}{R'_j} = \frac{p}{\sqrt{2/3}} \quad \text{and} \quad \frac{R_j}{x_j} = p, \quad j = 1, 2, 3. \quad (13)$$

Thus the  $x_j$ 's also denote the sides of  $\triangle_1$  with perimeter 1, similar to  $\triangle_p$  with the same orientation. The mapping of the spatial trajectory  $\mathbf{R}(t)$  to the planar trajectory  $\mathbf{x}(t)$  is one-to-one, provided that the radial projection of  $\dot{\mathbf{R}}$  onto  $\mathcal{P}$  is nonzero, or the spatial trajectory is not radial

$$\dot{\mathbf{R}} \times \mathbf{R} \neq 0. \quad (14)$$

This condition is fulfilled for the elliptic and hyperbolic cases. The condition can be violated only for the parabolic case, where the spatial trajectory can be radial. Then the radial projection of the trajectory onto  $\mathcal{P}$  reduces to one singular point  $\mathbf{q}$ . The loci of these singular points is called the critical curve  $\mathcal{C}$  such that each point  $\mathbf{q}$  on  $\mathcal{C}$  represents a  $\triangle_1$  corresponding to a radial trajectory of  $\triangle_P \sim \triangle_1$  either moving away from the origin with  $\dot{p} > 0$  or moving inward with  $\dot{p} < 0$ , see [2] and [5]. More details on the critical curve will be elaborated later in **Sec. 3**, to

set the stage for the main objective of the current paper, which is to identify branches of the critical curve that attract or repel nearby trajectories.

Due to the triangle inequality,

$$x_1 + x_2 \geq \frac{1}{2} \geq x_3, \quad x_2 + x_3 \geq \frac{1}{2} \geq x_1, \quad x_3 + x_1 \geq \frac{1}{2} \geq x_2, \quad (15)$$

$\mathbf{x}$  has to lie in the  $\Delta_Q$  with vertices  $Q_j$ ,  $j = 1, 2, 3$  lying at the midpoint of the  $j$ -th side of  $\Delta_{P_1P_2P_3}$ . The equality signs in (15) hold on the edges  $Q_1Q_2$ ,  $Q_2Q_3$  and  $Q_3Q_1$  of  $\Delta_Q$ , where  $x_3$ ,  $x_1$  and  $x_2 = 1/2$ , respectively, and the three vortices are collinear with the area of  $\Delta_p = 0$ . The vertex  $Q_j$  of  $\Delta_Q$  corresponds to a singular case where the three vortices degenerate to two. For example, at  $Q_1$ , where  $x_1 = 0$ , and  $x_2 = x_3 = 1/2$ , or  $R_1 = 0$  and  $R_2 = R_3$ , the three vortices degenerate to two, one at  $z_1$  with strength  $k_1$  and one at  $z_2 = z_3$  with strength  $k_2 + k_3$ .

On the positive (negative) face of the plane  $\mathcal{P}$ , or the  $\Delta_Q$ , where the normal vector to the face points away from (towards) the origin, we assign  $\gamma = 1$  ( $\gamma = -1$ ). With the same trilinear coordinates  $(x_1, x_2, x_3)$ , denoted by  $\mathbf{x}$ , the point on the positive (negative) face of  $\Delta_Q$  implies that the vertices of  $\Delta_1$ , or the three vortex centers  $z_1, z_2$  and  $z_3$  in the  $z$ -plane, are in the counterclockwise (clockwise) orientation, Fig. 1 (a) shows the vortex centers with  $\gamma = +1$ . We call the point  $\mathbf{x}$  on the negative side of  $\mathcal{P}$  the image of  $\mathbf{x}$  on the positive side and vice versa. The orientations of the vortex centers or  $\Delta_1$  can change only in crossing over an edge of  $\Delta_Q$ , where  $\Delta_1$  is collinear.

In trilinear coordinates, the two invariants (9) and (10) become,

$$[k_1^{-1}x_1^2 + k_2^{-1}x_2^2 + k_3^{-1}x_3^2]p^2 = a \quad \text{and} \quad (16)$$

$$x_1^{1/k_1} x_2^{1/k_2} x_3^{1/k_3} = bp^{K/(k_1k_2k_3)}. \quad (17)$$

With the elimination of the perimeter  $p$ , these two equations yield an integral curve, or a

trajectory, in  $\mathcal{P}$ , valid for all  $K$ . It is

$$\left[\frac{x_1^2}{k_1} + \frac{x_2^2}{k_2} + \frac{x_3^2}{k_3}\right]^{K/(2k_3)} [x_1^{1/k_1} x_2^{1/k_2} x_3^{1/k_3}]^{k_1 k_2} = \text{const.} \bar{I}. \quad (18)$$

For a parabolic case,  $K = 0$ , Eq. (18) reduces to

$$x_1^{k_2} x_2^{k_1} x_3^{k_1 k_2 / k_3} = \bar{I} \quad \text{or} \quad \left(\frac{x_1}{x_3}\right)^{k_2} \left(\frac{x_2}{x_3}\right)^{k_1} = \bar{I}, \quad (19)$$

which is equivalent to Eq. (17) for the parabolic case when the constant  $\bar{I}$  is identified as  $b^{k_1 k_2}$ . In the following subsection we recount the critical points in the planar trajectories first presented by Synge [2] with special attention to the parabolic cases.

### 2.3 Critical points $\mathbf{R}$ in space

It was shown in [2] that at a critical point  $\mathbf{R}$ , the configuration  $\Delta_p$  is stationary, i. e.,  $\dot{R}_j = 0$ ,  $j = 1, 2, 3$ , if and only if  $\Delta_p$  is either equilateral with  $R_1 = R_2 = R_3 = p/3$  or has zero area,  $|A| = 0$ . The latter requires that the configuration  $\Delta_1$  is collinear lying on an edge of  $\Delta_Q$  or at the vertices of  $\Delta_Q$ , where two vortices coincide to one, see Eqs. (8). These critical points of  $\mathbf{R}$  in space are also critical points  $\mathbf{q}$  in plane  $\mathcal{P}$ , or  $\mathbf{x}$  in the trilinear coordinates,  $x_1, x_2, x_3$  with  $p = 1$ , see Eqs. (13). An equilateral  $\Delta_p$ , implying  $x_1 = x_2 = x_3 = 1/3$  corresponds to the centroid  $E$  of  $\Delta_Q$  for positive orientation,  $\gamma = 1$  or its image  $E^*$  on the opposite side for  $\gamma = -1$ . For an equilateral configuration, it was shown that  $E$  and  $E^*$ , are stable for the elliptic case and unstable for the hyperbolic case [2]. For the parabolic case,  $E$  and  $E^*$  are degenerate singular points because they lie on the critical curve, which will be discussed in **Sec. 3**.

For a collinear configuration, the vortices  $z_j$ 's have to lie on a straight line,  $\mathcal{L}$ . Hence we could use real numbers  $s_j$  to locate  $z_j$  along  $\mathcal{L}$ , by setting  $s_1 = 0$  and assigning its direction such that  $s_2 = s_2 - s_1 = R_3 > 0$ . The condition of collinearity is

$$z_3 - z_1 = \nu(z_2 - z_1), \quad \text{or} \quad s_1 = 0, \quad s_2 = R_3 > 0, \quad s_3 = \nu s_2. \quad (20)$$

where  $\nu$  is a real number. The last equation implies  $R_2 = |\nu|R_3$ . From the values of  $\nu$ , whether negative, in  $[0, 1]$  or greater than 1, we see the relative positions of the vortices along  $\mathcal{L}$ , the collinear configurations and the locations of the critical points on the edges of  $\Delta_Q$  (see Fig. 2 and [5]). For Eq. (20) to hold for all  $t$ , we obtain from the equations of motion (4), that  $\nu$  has to be the root of the cubic equation,  $f(\nu) = 0$ , where

$$f(\nu) = (k_1 + k_2)\nu^3 - (k_1 + 2k_2)\nu^2 - (k_1 + 2k_3)\nu + (k_1 + k_3) \quad (21)$$

It was shown in [5], that there is a value  $K_* < 0$ , such that the cubic equation (21) has three unequal real roots for  $K > K_*$  and only one real root for  $K < K_* < 0$  in hyperbolic cases. For the parabolic cases, we have explicit formulas for the three roots of  $f(\nu) = 0$ . With  $k_3 = -k_1k_2/(k_1 + k_2)$ , we see that  $k_1/(k_1 + k_2)$  is a root of Eq. (21) and hence the three roots are:

$$\nu = k_1/(k_1 + k_2) \in [1/2, 1), \quad Q_6 \text{ on side } Q_1Q_2, \quad (22)$$

$$\nu = [k_2 - \sqrt{k_1^2 + k_1k_2 + k_2^2}]/(k_1 + k_2) < 0, \quad Q_4 \text{ on side } Q_2Q_3, \quad (23)$$

$$\nu = [k_2 + \sqrt{k_1^2 + k_1k_2 + k_2^2}]/(k_1 + k_2) > 1, \quad Q_5 \text{ on side } Q_3Q_1. \quad (24)$$

These three critical points lie on the respective sides of  $\Delta_Q$ .

The trajectories defined by Eq. (18) and the critical points were shown in Figs. 3, 4, and 5 in [5] for typical elliptic, hyperbolic and parabolic cases, respectively. In this paper we study the critical solutions, which occur only in the parabolic case; therefore, the figure for the parabolic case in [5] is reproduced here in Fig. 2.

It was noted before that a stationary point in the  $\mathbf{R}$  space corresponds to a stationary point  $\mathbf{q}$  on the plane  $\mathcal{P}$ , but the converse may not be true. A stationary point  $\mathbf{q}$  on  $\mathcal{P}$  could correspond to similar  $\Delta_p$  in the  $\mathbf{R}$  space with perimeter  $p(t)$  varying. Those stationary points on  $\mathcal{P}$  yields the critical curve  $\mathcal{C}$ . We shall examine in detail the geometry of the critical curve and the planar

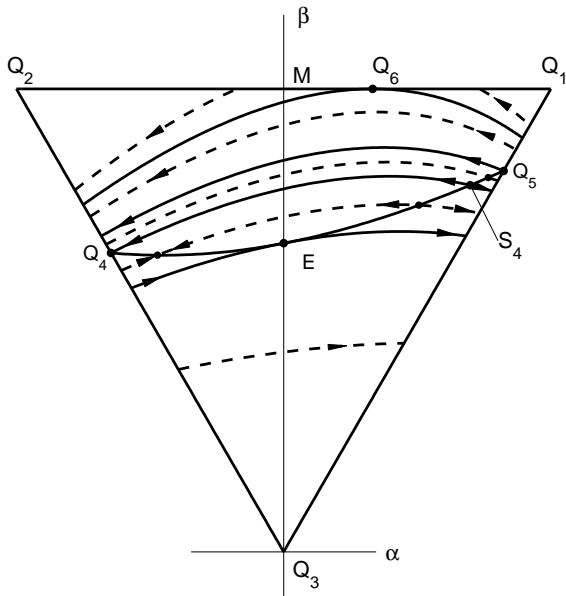


Figure 2: The trajectories for the parabolic case,  $k_1k_2 + k_2k_3 + k_3k_1 = 0$ , on the positive side of the plane  $\mathcal{P}$  or the equilateral  $\Delta_Q$ . That is, the configuration  $\Delta_1$  has counterclockwise orientation. Here  $k_1 = 2$ ,  $k_2 = 1$  and  $k_3 = -2/3$ . Also shown are the coordinates,  $\alpha\beta$ , with the vertex  $Q_3$  as the origin and  $Q_3E$  as the  $\beta$  axis.

trajectories, in particular those intersecting the critical curve, in the next section.

### 3 The planar trajectories and critical curve for the parabolic case

A point  $\mathbf{q}$  on the plane  $\mathcal{P}$ , represented by trilinear coordinates  $x_j$ ,  $j = 1, 2, 3$ , is related to the coordinates  $R_j$ ,  $j = 1, 2, 3$  of the point in space by Eq. (13). We have  $\dot{R}_j = p\dot{x}_j + x_j\dot{p}$ , and convert Eq. (8) for  $\dot{R}_j$  to equations for  $\dot{x}_j$  and  $\dot{p}$ . They are:

$$\dot{x}_1/x_1 = -\dot{p}/p + \gamma\mathcal{H}k_1(x_3^2 - x_2^2), \quad \dot{x}_2/x_2 = -\dot{p}/p + \gamma\mathcal{H}k_2(x_1^2 - x_3^2) \quad (25)$$

$$\dot{x}_3/x_3 = -\dot{p}/p + \gamma\mathcal{H}k_3(x_2^2 - x_1^2), \quad \text{where } \mathcal{H} = 2|A|/(p^2x_1^2x_2^2x_3^2), \quad (26)$$

$$\text{and } \dot{p}/p = \gamma \mathcal{H}[k_1 x_1(x_3^2 - x_2^2) + k_2 x_2(x_1^2 - x_3^2) + k_3 x_3(x_2^2 - x_1^2)]. \quad (27)$$

The last equation (27) follows either directly from Eq. (8) or from the sum of the preceding first three equations multiplied by  $x_j, j = 1, 2, 3$ , respectively.

We eliminate  $\dot{p}/p$  from the first three equations and obtain

$$\frac{\dot{x}_1}{x_1} - \frac{\dot{x}_2}{x_2} = -\frac{\gamma}{k_3} \mathcal{H}(\mathbf{x}) \mathcal{Y}(\mathbf{x}) \quad \text{and} \quad \frac{\dot{x}_1}{x_1} - \frac{\dot{x}_3}{x_3} = \frac{\gamma}{k_2} \mathcal{H}(\mathbf{x}) \mathcal{Y}(\mathbf{x}), \quad (28)$$

$$\text{where } \mathcal{Y}(\mathbf{x}) = k_2 k_3 x_1^2 + k_3 k_1 x_2^2 + k_1 k_2 x_3^2. \quad (29)$$

Using the identity,  $\sum_j x_j = 1$ , we get  $\sum_j \dot{x}_j = 0$ , and together with the two equations in (28) we solve for  $\dot{x}_1$ . We then get

$$\dot{x}_j = \gamma F_j \mathcal{H} \mathcal{Y} \quad (30)$$

$$\text{where } F_1 = x_1 \left[ \frac{x_3}{k_2} - \frac{x_2}{k_3} \right], \quad F_2 = x_2 \left[ \frac{x_1}{k_3} - \frac{x_3}{k_1} \right], \quad F_3 = x_3 \left[ \frac{x_2}{k_1} - \frac{x_1}{k_2} \right]. \quad (31)$$

To arrive at the same factor  $\mathcal{Y}(\mathbf{x})$  on the right hand sides of Eqs. (28) and (31), we used  $K = 0$ . Thus, the two linearly independent equations in (31) define the planar trajectory in  $\mathcal{P}$  for parabolic cases only. These two equations plus Eq. (27) for the variation of the perimeter are equivalent to the three equations (8) for the spatial trajectory in parabolic cases.

For points on  $\mathcal{C}$  other than the critical points  $Q_4, E, Q_5$  and  $E^*$  we have the common factor  $\mathcal{H} > 0$ . For all the points on  $\mathcal{C}$  to be stationary, it is necessary that the other common factor  $\mathcal{Y} = 0$ ,

$$\mathcal{Y}(\mathbf{x}) = k_2 k_3 x_1^2 + k_1 k_3 x_2^2 + k_1 k_2 x_3^2 = 0, \quad (32)$$

$$\text{or } Y(\mathbf{x}) = -\mathcal{Y}/k_3 = -k_2 x_1^2 - k_1 x_2^2 + (k_1 + k_2) x_3^2 = 0. \quad (33)$$

This is the equation for the critical curve  $\mathcal{C}$ , which exists only in the parabolic case.

Here the derivation of the equation for  $\mathcal{C}$  follows directly from the equations for  $\dot{x}_j$  in (31) and differs from the original derivation of Synge [2]. Besides being an alternative derivation,

the equations in (31) show explicitly the dependence of  $\dot{x}_j$ 's on  $\gamma$  and  $\mathcal{Y}$  or  $Y$ . That is *the direction of a trajectory is reversed when it crosses over an edge of  $\Delta_Q$  to the opposite side as  $\gamma$  changes from  $\pm 1$  to  $\mp 1$ , respectively, or when it crosses over the critical curve  $\mathcal{C}$ , where  $Y = 0$ , say from above to below as  $Y$  changes from positive to negative*. These results will be needed for our study of the trajectories in the strip containing the critical curve in **Subsecs. 3.1** and **3.2**.

On the stationary critical curve  $\mathcal{C}$ , the variation of the perimeter  $\dot{p}$  can be obtained directly from one of the equations in (25), say the first one. The result is

$$p^2(t) = p^2(0) + 4\gamma D_0 S_0 t, \quad (34)$$

$$\text{where } D_0 = \frac{x_2^2 - x_1^2}{k_1 k_2} \quad \text{and} \quad S_0 = \frac{\sqrt{(1-2x_1)(1-2x_2)(1-2x_3)}}{2k_1 k_2 k_3 (x_1 x_2 x_3)^2} \quad \text{are constants.} \quad (35)$$

We note that when  $p(t) = p(0)$ ,  $\mathbf{R}$  is stationary. This can happen only at the centroid  $E$  and its image  $E^*$  where  $x_1 = x_2 = x_3 = 1/3$  and  $D_0 = 0$  and at the critical points  $Q_4$  and  $Q_5$  on the two sides of  $\Delta_Q$  where  $|A| = 0$  and hence  $S_0 = 0$ . Thus the critical curve  $\mathcal{C}$  has to pass through  $E$  and  $E^*$  and cross over the sides  $Q_2Q_3$  and  $Q_3Q_1$  at the critical points  $Q_4$  and  $Q_5$ , respectively (see Eqs. (23) and (24)).

To describe the planar trajectories and the critical curve  $\mathcal{C}$  in the plane  $\mathcal{P}$ , i. e., to find their slopes and concavities, we need to replace the trilinear coordinates satisfying the constraint,  $x_1 + x_2 + x_3 = 1$ , by Cartesian coordinates in  $\mathcal{P}$ . We choose the coordinates  $\alpha$  and  $\beta$  with the vertex  $Q_3$  as the origin and the bisector of  $\angle Q_3$ ,  $Q_3EM$ , as the  $\beta$  axis, where  $M$  denotes the midpoint of the side  $Q_1Q_2$  (see Fig. 2), with

$$\beta = x_3 \quad \alpha = (x_2 - x_1)/\sqrt{3}, \quad \text{with inverse transformation,} \quad (36)$$

$$x_3 = \beta, \quad x_1 = [1 - \beta - \alpha\sqrt{3}]/2, \quad \text{and} \quad x_2 = [1 - \beta + \alpha\sqrt{3}]/2. \quad (37)$$

In terms of  $\alpha$  and  $\beta$ , Eq. (33) for  $\mathcal{C}$  becomes,

$$3\alpha^2 - 2\sqrt{3}\mu\alpha\beta - 3\beta^2 + 2\sqrt{3}\alpha - 2\beta + 1 = 0, \quad \text{where } \mu = (k_1 - k_2)/(k_1 + k_2). \quad (38)$$



It is a hyperbola. Its intercept with the  $\beta$  axis is given by the equation  $3\beta^2 + 2\beta - 1 = 0$ , which has one root,  $\beta = x_3 = 1/3$  while  $x_1 = x_2 = (1 - x_3)/2 = 1/3$ , representing the point  $E$  or its image  $E^*$ . The second root,  $\beta = -1$  should be excluded because  $\beta = x_3$  cannot be negative. Thus the critical curve  $\mathcal{C}$  should be the upper branch of the hyperbola (38) inside  $\Delta_Q$ , which is concave upward in the  $\alpha\beta$  plane and passes through the centroid  $E$  (or  $E^*$  on the negative side).

The curve  $\mathcal{C}$  intersects the side  $Q_3Q_1$  at point  $\mathbf{x}$  where  $x_2 = 1/2 = x_1 + x_3$ , and Eqs. (20) and (24) yield the equations for  $x_3$  and  $x_1 \in (0, 0.5)$ ,

$$x_3 = \frac{\sqrt{k_1^2 + k_2^2 + k_1k_2} - k_2}{2k_1}, \quad \text{and} \quad x_1 = \frac{1}{2} - x_3 = \frac{k_1 + k_2 - \sqrt{k_1^2 + k_2^2 + k_1k_2}}{2k_1}. \quad (39)$$

Likewise,  $\mathcal{C}$  intersects the side  $Q_2Q_3$  at the critical point  $Q_4$  defined by Eqs. (20) and (23).

Thus  $\mathcal{C}$  is divided by  $Q_4, E, Q_5$  and  $E^*$  into four branches;  $Q_4E$  and  $EQ_5$  on the positive side of  $\mathcal{P}$  and their images  $Q_5E^*$  and  $E^*Q_4$  on the negative side. From Eq. (3), we have  $S_0 < 0$  when  $A \neq 0$ , hence  $\dot{p}$  has the same sign as  $-\gamma C_0$ , i. e., the same sign as  $\gamma(x_1 - x_2)$ . On the positive side of  $\mathcal{P}$ ,  $\gamma = 1$ , we have  $\dot{p} < 0$  on the branch  $EQ_5$  where  $x_1 < x_2 < 1/2$  and  $\dot{p} > 0$  on the branch  $Q_4E$ , where  $x_2 < x_1 < 1/2$ . On the negative side,  $\gamma = -1$ , the sign of  $\dot{p}$  on the images of the branches is reversed. Thus the points in the branches  $Q_4E$  and  $E^*Q_5$ , excluding their end points, correspond to expanding similar configurations  $\Delta_p$  while those in  $EQ_5$  and  $E^*Q_4$  correspond to contracting similar configurations. It was observed before from Eq. (34) that the perimeter  $p$  remains stationary at the end points  $Q_4, E, Q_5$  and  $E^*$  and the corresponding vortex configuration  $\Delta_p$  or  $\mathbf{R}$  remains stationary also.

Now we study the slopes and concavities of the trajectories, along constant  $\bar{I}$  curves. From those integral curves intersecting the critical curve  $\mathcal{C}$ , we find the variation of the invariant  $\bar{I}$  along  $\mathcal{C}$  and then define the boundary of the strip containing  $\mathcal{C}$ . For this purpose, it suffices to study only the positive side of  $\mathcal{P}$ , where  $\gamma = +1$ . We note that the slope of a point on the

critical curve in the  $\mathcal{P}$  or  $\alpha\beta$ -plane, is defined by,

$$d\beta/d\alpha = (k_1x_2 - k_2x_1)\sqrt{3}/[2(k_1 + k_2)x_3 + k_2x_1 + k_1x_2]. \quad (40)$$

The slope has the same sign as the factor  $(k_1x_2 - k_2x_1)$ . In the  $\alpha\beta$  plane, the curve  $\mathcal{C}$  is concave upward with the minimum  $\beta$  or  $x_3$  at  $x_2 = k_2x_1/k_1 \leq x_1$ . This is in agreement with Eq. (38), which says that  $\mathcal{C}$  is the upper branch of a hyperbola passing through  $E$ .

For a trajectory in the parabolic case, Eq. (19), its slope is,

$$m = d\beta/d\alpha = \sqrt{3}x_3(k_1x_1 - k_2x_2)/[2(k_1 + k_2)x_1x_2 + (k_1x_1 + k_2x_2)x_3]. \quad (41)$$

The slope  $m$  has the same sign as the factor  $(k_1x_1 - k_2x_2)$ , so the trajectory is concave downward with the maximum  $\beta$  at  $x_2 = k_1x_1/k_2 \geq x_1$  where  $\alpha > 0$ .

As  $\beta$  increases from 0 to  $1/2$ , the invariant  $\bar{I}$  decreases from  $\infty$  monotonically along radial lines from  $Q_3$ , the origin,  $\alpha = 0, \beta = 0$ . Thus the corresponding trajectories move upward as  $\bar{I}$  decreases.

Since the critical curve  $\mathcal{C}$  is concave upward while the trajectories are concave downward,  $\mathcal{C}$  comes in contact with the first trajectory when they are tangent to each other. This happens at point  $E$  on  $\mathcal{C}$  with a trajectory with  $\bar{I} = 1$  with common slope

$$d\beta/d\alpha = (k_1 - k_2)/[(k_1 + k_2)\sqrt{3}] \geq 0. \quad (42)$$

That is, the trajectories with  $\bar{I} > 1$  remain below  $\mathcal{C}$  and the one with  $\bar{I} = 1$  is tangent to  $\mathcal{C}$  at the centroid  $E$ . This statement holds for the images of the trajectories and the critical curve on the negative side of  $\mathcal{P}$ . Hence *the trajectory with  $\bar{I} = 1$  on both sides of  $\mathcal{P}$  is the lower boundary of a strip  $\mathcal{S}$  containing  $\mathcal{C}$ . On the other hand, The trajectory with  $\bar{I} = 1$  encloses all the trajectories with  $\bar{I} > 1$ , which are the periodic orbits around the center  $Q_3$ .*

As  $\bar{I}$  decreases from 1, the trajectory will intersect  $\mathcal{C}$  at two points on the left branch  $Q_4E$  and the right branch  $EQ_5$ , respectively. To find the upper boundary trajectory of the strip  $\mathcal{S}$ ,

we need to find whether it is the trajectory passing through  $Q_4$  or  $Q_5$  by comparing the values of their invariants  $\bar{I}(Q_4)$  and  $\bar{I}(Q_5)$ . For this comparison, we use  $\bar{I}_j$  to denote  $\bar{I}(Q_j)$ . Let the  $x_3$  coordinates of  $Q_4$  and  $Q_5$  be denoted by  $\beta_4$  and  $\beta_5$ , then we have

$$\bar{I}_4 = \bar{I}(Q_4) = (2\beta_4)^{-(k_1+1)}(1-2\beta_4)^{k_1}, \quad \text{and} \quad \bar{I}_5 = \bar{I}(Q_5) = (2\beta_5)^{-(k_1+1)}(1-2\beta_5)^{k_1}, \quad (43)$$

with  $k_2 = 1$  according to Eq. (3). From the  $x_3$ 's for  $Q_4$  and  $Q_5$ , Eq. (39), we have

$$2\beta_4 = (k_1 + 1)/(q + k_1) \quad \text{and} \quad 2\beta_5 = (k_1 + 1)/(q + 1), \quad (44)$$

where  $q = \sqrt{k_1^2 + k_1 + 1} \geq \sqrt{3}$  and the ratio,

$$f(k_1) = \bar{I}_4/\bar{I}_5 = [(q-1)/(q+1)]^{k_1} [(q+k)/(q-k)] > 0. \quad (45)$$

When  $k_1 = k_2 = 1$ , the integral curves are symmetric with respect to the  $\beta$ -axis, the bisector of  $\angle Q_3$ . In particular, we have  $\beta_5 = \beta_4$ ,  $f = 1$  or  $\bar{I}_4 = \bar{I}_5$ , and the trajectory through  $Q_4$  coincides with that through  $Q_5$ .

With  $k_1 > k_2 = 1$ , we shall show the ratio,  $f(k_1) = \bar{I}_4/\bar{I}_5 \geq 1$  for  $k_1 \geq 1$ . With  $f(1) = 1$ , we need only prove  $df/dk_1 > 0$ , or rather  $d \ln f/dk_1 > 0$ . With  $2qdq/dk = 2k_1 + 1$ , we have

$$d \ln f/dk_1 = -\ln[(1+\nu)/(1-\nu) + 2\nu + \nu(k_1^2\nu^2)/(1-\nu^2)], \quad (46)$$

where  $\nu = 1/q$ . As  $k_1$  increases from 1 to  $\infty$ ,  $q$  increases from  $\sqrt{3}$  to  $\infty$ ,  $\nu$  decreases from  $1/\sqrt{3}$  to 0 and  $(1-\nu^2)^{-1}$  decreases from  $3/2$  to 1. The curve  $y = (1-x^2)^{-1}$  is concave upward and intersects the straight line or the chord,  $y^+ = 1 + [x\nu/(1-\nu^2)]$ , at points  $(0, 1)$  and  $(\nu, (1-\nu^2)^{-1})$ . That is, the curve lies below the chord,  $y^+ > y$ , for  $x \in (0, \nu)$ . Thus we have

$$\frac{2-\nu^2}{2(1-\nu^2)} = \frac{1}{\nu} \int_0^\nu y^+ dx > \frac{1}{\nu} \int_0^\nu \frac{dx}{1-x^2} = \frac{1}{2\nu} \ln \frac{1+\nu}{1-\nu} \quad (47)$$

Equation (46) becomes

$$d \ln f/dk_1 = [(2-\nu^2)\nu/(1-\nu^2) - \ln[(1+\nu)/(1-\nu)]] + (k_1^2 - 1)\nu^3/(1-\nu^2) > 0, \quad (48)$$

$$\text{and hence} \quad \bar{I}(Q_4) \geq \bar{I}(Q_5) \quad \text{or} \quad \bar{I}_4 \geq \bar{I}_5, \quad \text{for} \quad k_1 \geq 1 \quad (49)$$

The equality sign holds only when  $k_1 = 1 = k_2$ . This completes the proof, which was omitted in the 1988 paper [5]. Note that the trajectory through  $Q_4$  lies in the strip  $\mathcal{S}$ , above the lower trajectory through  $E$  and below the upper one through  $Q_5$  as shown in Fig. 2.

For the trajectories with  $\bar{I} \in (\bar{I}_6, \bar{I}_5)$ , they will remain above  $\mathcal{C}$  and cross over to the opposite side of  $\mathcal{P}$  to form periodic orbits. For  $\bar{I} = \bar{I}_6$ , the trajectory becomes the separatrix through the critical point  $Q_6$  on the side  $Q_1Q_2$ , as shown in Fig. 2. For  $\bar{I} \in (0, \bar{I}_6)$  the trajectories will either be periodic orbits around the center  $Q_1$  or the center  $Q_2$ . This completes the description of the trajectories, separatrices and the critical curve in a parabolic case shown in Fig. 2, which was presented in [5].

From Eqs. (49) and (42), we see that *on the positive side of  $\mathcal{P}$ , the critical curve  $\mathcal{C}$  is contained in a strip  $\mathcal{S}$ , bounded above by the trajectory through point  $Q_5$  on edge  $Q_3Q_1$  with  $\bar{I} = \bar{I}_5$  and below by the trajectory through the centroids,  $E$  and  $E^*$ , with  $\bar{I} = 1$ . Thus the strip  $\mathcal{S}$  contains besides  $\mathcal{C}$  all trajectories with  $\bar{I} \in [\bar{I}_5, 1]$ . Likewise, we define the image of the strip on the negative side of  $\mathcal{P}$ .*

In the next subsection we will find out whether a trajectory through a point near  $\mathcal{C}$  will be attracted to a point  $\mathbf{q}$  on  $\mathcal{C}$  or depart from  $\mathbf{q}$  with increasing time.

### 3.1 Trajectories in the strip $\mathcal{S}$ containing $\mathcal{C}$

Note that a point on the critical curve  $\mathcal{C}$  is a stationary point. A trajectory will either stay above  $\mathcal{C}$  or below  $\mathcal{C}$  but *will not cross over  $\mathcal{C}$* . Thus  $\mathcal{C}$  partitions the strip  $\mathcal{S}$  on the positive side of  $\mathcal{P}$  into two strips  $\mathcal{S}^+$  and  $\mathcal{S}^-$  above and below  $\mathcal{C}$ . To find out whether a trajectory through a point in the neighborhood of  $\mathcal{C}$  will depart from or be attracted to  $\mathcal{C}$ , we need to know the direction along the trajectory as  $t$  increases. For this, we use Eqs. (31). We see that  $\dot{x}_1$  and  $\dot{x}_2$  changes signs only when crossing over an edge where  $\gamma$  changes sign or over  $\mathcal{C}$  where

$\mathcal{Y}$  does. The factor  $F_1 > 0$  and  $F_2 < 0$  so that they contribute to a factor in  $\dot{\alpha} < 0$  because it has the same sign as that  $F_2 - F_1$ . That is the  $\dot{\alpha}$  will have the same sign as  $\dot{x}_2$  and change its sign in crossing over an edge or over  $\mathcal{C}$ . For  $\dot{x}_3$  or  $\dot{\beta}$ , we see there is an addition sign change because the factor  $F_3$  can cross over zero. This sign change in  $\dot{\beta}$  defines the concavity of the trajectory, concaving downward, and the maximum of  $\beta$ . Thus the directivity of the trajectories are defined by Eq. (31). For  $j = 3$  we obtain

$$\dot{\beta} = \dot{x}_3 = \gamma \mathcal{H} \mathcal{Y} x_3 \left[ \frac{k_2 x_2 - k_1 x_1}{k_1 k_2} \right]. \quad (50)$$

and  $\beta$  or  $x_3$  reaches its maximum when  $k_2 x_2 = k_1 x_1$  as expected from Eq. (41) for the slope  $m = 0$ . From the concavities of the trajectories and the critical curve, we showed in the preceding subsection that a trajectory with  $\bar{I} \in [\bar{I}_4, 1)$  will intersect  $\mathcal{C}$  twice in  $\mathcal{S}^+$  on the positive side of  $\mathcal{P}$  and cross over the two edges in  $\mathcal{S}_-$  at the expanding branch,  $Q_4 E$  to the left of the centroid  $E$ , where  $x_1 > x_2$  with slope  $m > 0$  and at the contracting branch  $E Q_5$  to the right of  $E$  where  $x_2 > x_1$  with  $m < 0$ . A trajectory with  $\bar{I} \in [\bar{I}_5, \bar{I}_4)$  will intersect only the right branch  $E Q_5$  of  $\mathcal{C}$  and cross over the left edge in  $\mathcal{S}^+$  and the right edge in  $\mathcal{S}^-$ . From Eq. (31), we see that on the positive side of  $\mathcal{P}$ ,  $\gamma = 1$ , and  $\dot{\beta}$  has the same sign as  $\mathcal{Y}[k_1 x_1 - k_2 x_2]$  or the opposite sign of  $m \mathcal{Y}$  since  $\mathcal{H} > 0$ .

Recalling that  $\mathcal{Y} > 0$  when the point is above  $\mathcal{C}$ , and  $\mathcal{Y} < 0$  when below, we have the direction of a trajectory near  $\mathcal{C}$  on the positive side of  $\mathcal{P}$ ,

$$\text{Near the branch } EQ_5, \quad m > 0, \quad \dot{\beta} > 0 \text{ above } \mathcal{C}, \quad (51)$$

$$\dot{\beta} < 0, \text{ below } \mathcal{C}, \quad (52)$$

$$\text{Near the branch } Q_4 E, \quad m < 0, \quad \dot{\beta} < 0 \text{ above } \mathcal{C}, \quad (53)$$

$$\dot{\beta} > 0, \text{ below } \mathcal{C}. \quad (54)$$

On the negative side of  $\mathcal{P}$ ,  $\gamma = -1$ , the inequality signs will be reversed. The directions of the

trajectories shown in Fig. 2 are in agreement with the statements above. These statements say that

*In the neighborhood of a contracting (expanding) branch,  $EQ_5$  or  $Q_4E^*$  ( $Q_4E$  or  $E^*Q_5$ ), a trajectory will depart from (be attracted to)  $\mathcal{C}$ .*

It is equivalent to say that

*When the initial vortex configuration similar to  $\Delta_1$  or point  $\mathbf{q}$  on a contracting branch of the critical curve  $\mathcal{C}$  is disturbed off  $\mathcal{C}$ , the trajectory will depart from  $\mathcal{C}$  and finally be attracted to an expanding branch of  $\mathcal{C}$ .*

In particular, *Contracting similar vortex configuration,  $\Delta_p$  leading to coalescence of the three vortices is a theoretical solution but unlikely to happen.*

Knowing the directivities of the trajectories, we shall describe in the following subsection how the trajectories in the strip  $\mathcal{S}$  depart from a contracting or unstable branch of  $\mathcal{C}$  ending on an expanding or stable branch and classify the trajectories into three types.

### 3.2 Departure from a contracting branch of the critical curve

For the region  $\mathcal{S}^-$ , the centroid  $E$  divides it into two with  $x_2 > x_1$  and  $x_2 < x_1$  respectively. Likewise the image of  $\mathcal{S}_-$  is divided by  $E^*$  into two. We use  $\mathcal{S}_R^-$  to denote the subregion of  $\mathcal{S}^-$  where  $x_2 > x_1$ , bounded above by the contracting branch  $EQ_5$  and below by the trajectory with  $\bar{I} = 1$  on the positive side of  $\mathcal{P}$  and is connected across the edge where  $x_2 = 0.5$  to its image on the negative side of  $\mathcal{P}$  in which the upper boundary is the expanding branch  $Q_5E^*$ . A trajectory in  $\mathcal{S}_R^-$  with  $\bar{I} \in (\bar{I}_5, 1)$  will depart from a point below the contracting branch  $EQ_5$  cross over to edge and be attracted to the expanding edge  $E^*Q_5$ . Likewise, we use  $\mathcal{S}_L^-$  to denote the corresponding region where  $x_2 < x_1$ . The trajectories  $\mathcal{S}_L^-$  have  $\bar{I} \in (\bar{I}_4, 1)$  would depart from the contracting branch  $E^*Q_4$  and be attracted to the expanding branch  $Q_4E$ . The

trajectories in  $\mathcal{C}^-$  are classified as trajectories of type I.

For the region  $\mathcal{S}^+$  above  $\mathcal{C}$ , Eq. (49) says that there is a separatrix from  $Q_4$  which intersects  $\mathcal{C}$  at  $S_4$  and partitions the branch  $EQ_5$  into  $ES_4$  and  $S_4Q_5$  and also the strip  $\mathcal{S}^+$  into two strips  $\mathcal{S}_4^+$  and  $\mathcal{S}_5^+$  with  $\bar{I} \in (\bar{I}_4, 1)$  and  $\in (\bar{I}_4, \bar{I}_5)$ , respectively (see Fig. 2).

For a  $\bar{I} \in (\bar{I}_4, 1)$ , the trajectory in  $\mathcal{S}_4^+$  on the positive side of  $\mathcal{P}$  intersects  $\mathcal{C}$  at two points on the left branch  $Q_4E$  and the right branch  $ES_4$ , respectively, i. e., it remains on the positive side. The same holds for its image on the negative side. The trajectory in  $\mathcal{S}_4^+$  and its image are of type II (see Fig. 2).

For a  $\bar{I} \in (\bar{I}_5, \bar{I}_4)$ , the trajectory in  $\mathcal{S}_5^+$  in the positive part of  $\mathcal{P}$  will be above  $\mathcal{C}$ , cross over the edge  $Q_2Q_3$  and continue along the image of the trajectory in the reverse direction. The trajectories in  $\mathcal{S}_5^+$  are classified as type III (see Fig. 3).

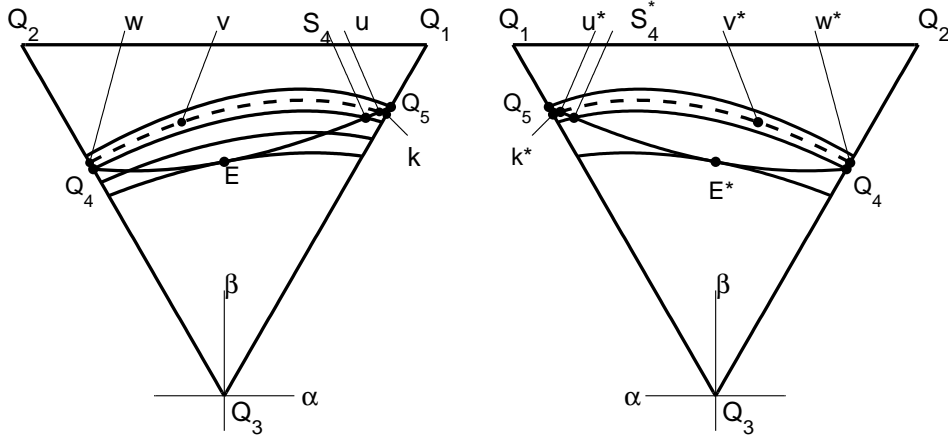


Figure 3: Departure from a point,  $u$  or  $u^+$ , on an unstable branch  $EQ_5$  of the critical curve along the trajectory  $u - v - w$  in the plane  $\mathcal{P}$ , with  $\gamma = +1$  and along its image  $w - v^* - u^* - u_c$  in  $\mathcal{P}$  with  $\gamma = -1$ . The last point  $u_c$  denotes the point where the trajectory intersects the stable branch  $E^*Q_5$  of  $\mathcal{C}$ .

The above theoretical predictions and classifications of the trajectories in the strip  $\mathcal{S}$  will

be illustrated or confirmed by the numerical examples in the next section.

## 4 Numerical Simulations

In this section, we present numerical examples to simulate or substantiate the conclusions arrived at in Subsec. 3.2 via the directivity of the trajectories intersecting the critical curve  $\mathcal{C}$ . That is, a configuration or a point  $\mathbf{x}$  in the neighborhood of a contracting branch of  $\mathcal{C}$  will depart from  $\mathcal{C}$  along a trajectory with constant integral invariant  $\bar{I}$  and end on an expanding branch of  $\mathcal{C}$ . Instead of integrating the governing equations (8) for the vortex configurations from the initial configuration, the numerical examples are based on the integration of the primary equations of motion of the three vortices, Eqs. (4) in the  $z$ -plane with initial data  $z_j(0)$ 's corresponding to the initial configuration  $\Delta_1$ 's in the neighborhood of  $\mathcal{C}$ .

First we prescribe the strengths of the three vortices belonging to the parabolic case: with  $k_2 = 1$  as the scale for the strength, we choose  $k_1 = 2$  and get  $k_3 = k_1 k_2 / (k_1 + k_2) = -2/3$ . Without losing generality, we choose the initial perimeter of  $\Delta_p$  to be the length scale, i. e.,  $p(0) = 1$  and hence  $R_j(0) = x_j(0)$ .

To carry out the integration of the primary equations (4), we shall relate the initial positions of the vortices<sup>1</sup>  $z_j(0)$ 's to the initial configuration,  $R_j(0) = x_j(0)$  by (i) aligning  $z_1$  and  $z_2$  parallel to the imaginary axis, i. e., setting  $\Re z_1 = \Re z_2$ , (ii) requiring  $\Im z_1 > \Im z_2$  and  $\Re z_3 > \Re z_1$ , so that the configuration  $\Delta_1$  is oriented counterclockwise,  $\gamma = +1$ , and (iii) putting the stationary center of vorticity at the origin,  $z = 0$ . The relationships for the initial data with  $R_j(0) = x_j(0)$  are:

$$|z_3 - z_1|^2 = R_2^2 \quad |z_2 - z_3|^2 = R_1^2 \quad (55)$$

$$z_1 - z_2 = iR_3 \quad \text{and} \quad k_1 z_1 + k_2 z_2 + k_3 z_3 = 0. \quad (56)$$

---

<sup>1</sup>Note that  $x_j$ ,  $j = 1, 2, 3$  denote the trilinear coordinates and should not be confused with  $\Re z_j$ .



Case	$R_1$	$R_2$	$R_3$	$Y(0)$	$\bar{I}(0)$
$r_-$	0.18195	0.44396	0.37409	-0.00498	0.68503
$r_+$	0.19108	0.43424	0.37468	0.00501	0.68500
$u_-$	0.10442	0.49225	0.40333	-0.00500	0.38563
$u_+$	0.10839	0.48643	0.40518	0.00502	0.38555

Table 1: Specification of numerical examples. In all cases,  $k_1 = 2$ ,  $k_2 = 1$ , and  $k_3 = -2/3$ .

From Eq. (55) and the imaginary parts of the equations in (56), we get  $\Im z_j(0)$ ,

$$\Im z_2 = [-k_3(R_1^2 - R_2^2) + R_3^2(2k_1 + k_3)]/[2R_3(k_1 + k_2 + k_3)], \quad (57)$$

$$\Im z_1 = \Im z_2 + x_3 \quad \text{and} \quad \Im z_3 = -[k_1 \Im z_1 + k_2 \Im z_2]/k_3 \quad (58)$$

By equating the real parts of the equations in (56), we get

$$\Re z_1 = \Re z_2, \quad \Re z_3 - \Re z_1 = \sqrt{R_2^2 - (\Im z_3 - \Im z_1)^2} \quad \text{and} \quad (k_1 + k_2)\Re z_1 + k_3\Re z_3 = 0. \quad (59)$$

These three equations in turn define  $\Re z_j(0)$ . With those initial data, we carry out numerical integration of the primary equations (4), obtain the motions of the vortices,  $z_j(t)$ 's, and recover the vortex configuration, the sides  $R_j(t)$  and the perimeter  $p(t)$  of  $\Delta_p(t)$ , and then the three sides,  $x_j(t) = R_j/p$  of  $\Delta_1(t)$ .

Ten numerical examples were carried out and the results concurred with the theoretical conclusions that a configuration slightly perturbed from a contracting branch of the critical curve  $\mathcal{C}$  will depart from  $\mathcal{C}$  and end on an expanding branch of  $\mathcal{C}$  belonging to one of the three types described in Subsec. 3.2. Here we shall present only four typical numerical examples. Table 1 gives the four sets of initial configurations,  $R_j(0) = x_j(0)$  with  $p(0) = 1$  and the corresponding values of  $Y(0)$  and the invariant  $\bar{I}(0)$  defined by Eqs (33) and (18), respectively.

Since the critical curve  $\mathcal{C}$  is defined by  $Y(x_j) = 0$ , see Eq. (29), the deviation of point  $x_j$

from  $\mathcal{C}$  is measured by  $Y(x_j)$  with  $Y$  positive (negative) for  $x_j$  lying above (below) the critical curve.

The contracting branch  $EQ_5$  of  $\mathcal{C}$  on the positive side of the plane  $\mathcal{P}$  is composed of segments  $ES_4$  and  $S_4Q_5$  with invariant  $\bar{I}$  decreasing respectively from  $\bar{I}(E) = 1$  to  $\bar{I}_4$  and from  $\bar{I}_4$  to  $\bar{I}_5$ . See Figs. 2 and 3.

The integral invariants  $\bar{I}(0)$ 's in the table define the locations of the critical points on the contracting branch of  $\mathcal{C}$  and each shall remain constant for  $t > 0$  along the trajectory towards an expanding branch of  $\mathcal{C}$ .

The first and second rows of data in Table 1 list the initial data corresponding to point  $r^\mp$  perturbed below and above, respectively. from point  $r$  in the segment  $ES_4$  of  $\mathcal{C}$ . Likewise, the third and fourth rows list the initial data corresponding to points  $u^\mp$  perturbed from a point  $u$  in the segment  $S_4Q_5$  of  $\mathcal{C}$ .<sup>2</sup>

For each case, the integral invariant  $\bar{I}(t)$  differs from its initial value  $\bar{I}(0)$  by less than 0.1%, that is, the numerical solution  $z_j(t)$  does yield a planar trajectory of constant  $\bar{I}(0)$ .

Figures 4, 5 and 6 show, respectively, the variations of the perimeter,  $\log p(t)$ , the deviation from the critical curve,  $Y(t)$ , and the vortex configuration scaled by its perimeter,  $\Delta_1$ , along the trajectories for the four cases listed in Table 1.

When a trajectory crosses over an edge to the opposite side of  $\mathcal{P}$ , i. e.,  $\gamma$  changes from  $\pm 1$  to  $\mp 1$ , it continues along the image of that on the positive side but in reverse direction; therefore, at an edge,  $\log p$  reaches an extremum and so does  $Y$  while the three vortices become collinear. We also note that on either side of  $\mathcal{P}$  or the  $\alpha\beta$  plane, the trajectories,  $\bar{I} = \text{constant}$ , are concave downward while the constant  $Y(x_j)$  lines are concave upward similar to that of  $\mathcal{C}$  where  $Y = 0$ .

---

<sup>2</sup>The  $x_j$ 's of point  $r$  on  $\mathcal{C}$ , where  $Y = 0$  can be defined from the linear interpolation of  $x_j$ 's of  $r^\pm$  with respect to  $Y^\pm(0)$ . Likewise we can locate the  $x_j$ 's of point  $u$  on  $\mathcal{C}$  from those of  $u^\pm$ .

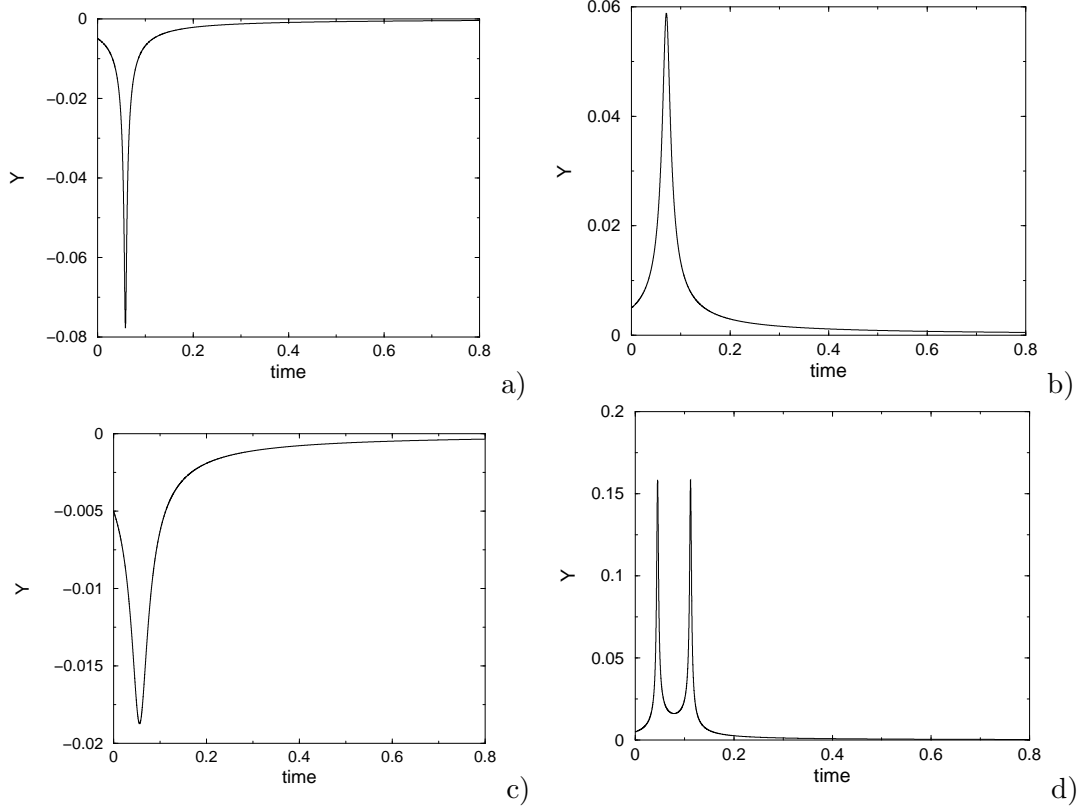


Figure 4: Variation of  $Y(\mathbf{x})$  along a trajectory,  $\mathbf{x}(t)$ , departing from an unstable branch of the critical curve to a stable branch. Point of departure:  $r^-$ ,  $r^+$ ,  $u^-$ , and  $u^+$  in a), b), c) and d).

The trajectory  $\bar{I} = 1$  and the critical curve  $Y = 0$  are of opposite concavity. They are tangent to each other at  $E$  (or  $E^*$ ). The trajectories intersecting the left (right) branch  $Q_4E$  or  $EQ_5$  of  $\mathcal{C}$  will have  $\bar{I}(Q_4) < \bar{I} < 1$  or  $\bar{I}(Q_5) < \bar{I} < 1$ . This statement holds also for the images of the trajectories.

The trajectories with  $\bar{I} < 1$  will be tangent to a constant  $Y$ -line with  $Y > 0$  above  $\mathcal{C}$ . Thus along a trajectory with  $\bar{I} < 1$ ,  $Y(\mathbf{x})$  reaches a maximum at a point above  $\mathcal{C}$ . Again this holds also for the image trajectory on the negative side of  $\mathcal{P}$

Along a trajectory initiating at point below  $\mathcal{C}$ , say  $r^-$  or  $u^-$ , the deviation,  $\delta = -Y$ , (the perimeter or  $-\log p$ ) will increase from almost zero, or  $\delta \ll 1$ , to a maximum at the edge and then return to zero as the trajectory ending at a point on the stable branch of  $\mathcal{C}$  while  $\Delta_1(t)$

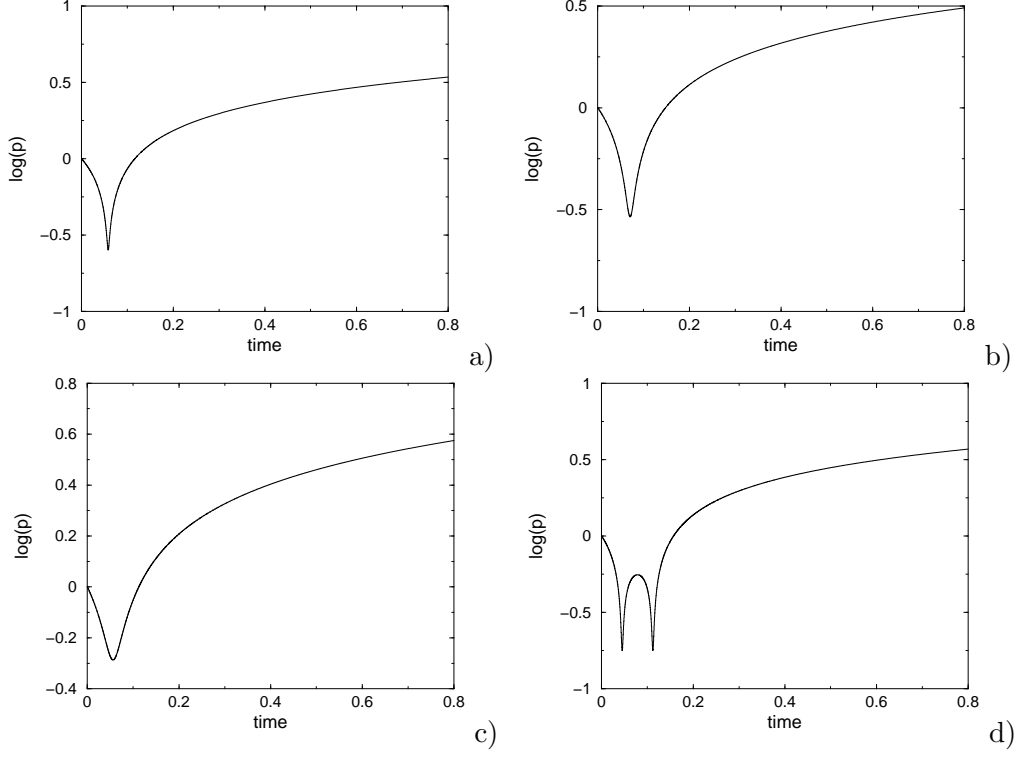


Figure 5: Variation of  $\log p(\mathbf{x})$  along a trajectory,  $\mathbf{x}(t)$ , departing from an unstable branch of the critical curve to a stable branch. Point of departure:  $r^-$ ,  $r^+$ ,  $u^-$ , and  $u^+$  in a), b), c) and d).

becomes equivalent to  $\Delta_1(0)$  with a change of orientation. The trajectory is of type I. See part a) and c) of these three figures.

For a trajectory initiating from a point, say  $r^+$ , above the unstable branch  $ES_4$  of  $\mathcal{C}$  where  $\bar{I}(S_4) = \bar{I}(Q_4) > \bar{I}(Q_5)$ , the deviation  $\delta$  will increase from a small initial value,  $\ll 1$ , to a maximum and then return to zero as the trajectory arrives at a point on the stable branch  $Q_4E$  of  $\mathcal{C}$  without crossing over an edge, i. e., staying on the same side of  $\mathcal{P}$ , as in Fig. 4 b). The trajectory is of type II. The perimeter will decrease from 1 to a minimum and then keep on increasing as  $t$  increases. See part b) in Fig. 5. Note that the final configuration corresponding to the point on the left branch  $Q_4E$  is different from the initial one on the right branch  $ES_4$ , as shown in Fig. 6 d).

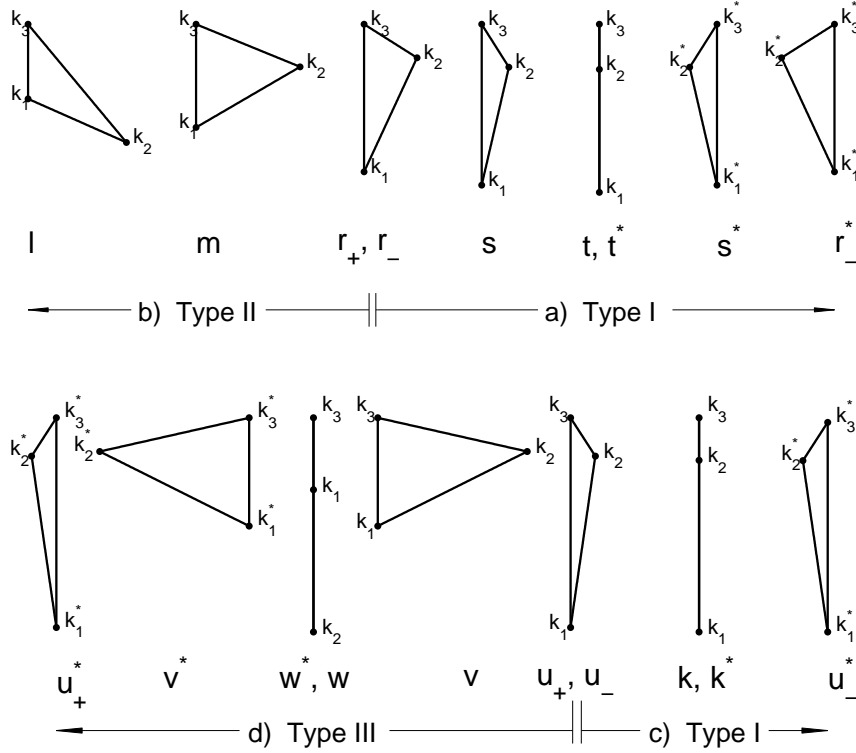


Figure 6: Evolution of  $\Delta_1$  departing from the unstable branch on the positive side of  $\mathcal{P}$  to the stable branch on the negative side of type I or III, or to that on the positive side of type II.

For a trajectory initiated from a point,  $u^+$  above  $\mathcal{C}$  with  $\bar{I} \in (\bar{I}(Q_5), \bar{I}(Q_4))$ , the deviation,  $\delta = Y(0)$ , will increase from a small initial value  $\ll 1$  to a maximum, crossing the edge  $Q_2Q_3$  with  $Y$  reaching a local minimum and continue to the negative side of  $\mathcal{P}$  with  $Y$  appearing as the image of the first part passing through the image point of  $u^+$ , then return to zero as it reaches a point on the stable branch of  $\mathcal{C}$ . The image of the point will be close to the initial point  $u^+$ . The trajectory is of type III.

Our numerical examples show the three distinct types of trajectories expected in the theoretical studies in the preceding section. Note that the deviation  $Y(t)$  and the perimeter  $p(t)$  for type III have three extrema as  $t$  increases while those for type I and II have only one. For type I and III, there are changes of orientation and the final configurations are nearly similar

to the original ones with perimeter increasing. For type II, there are no changes of orientation but the final expanding configuration is not similar to the initial one.

The trajectories depart from the unstable branch  $E^*Q_4$  of  $\mathcal{C}$  on the negative side of  $\mathcal{P}$ . Because of  $\bar{I}_4 > \bar{I}_5$ , the departing trajectories are only of two types: trajectories of type I begin from a point below the branch  $Q_4E^*$  while those of type II begin from a point above.

## 5 Conclusion

This paper presents a complete description of the global dynamics of three point vortices initially in the neighborhood of the planar critical curve  $\mathcal{C}$  in trilinear coordinates  $x_j$ ,  $j = 1, 2, 3$ . The trilinear coordinates, only two of which are independent because of the constraint  $x_1 + x_2 + x_3 = 1$ , were introduced by Synge (1949) to study the deformation of the triangle  $\Delta_p$  formed by the three vortices with sides  $R_j$  and perimeter  $p$  via that of a similar triangle with sides  $x_j$  and perimeter one. A spatial trajectory  $R_j(t)$  is then reduced to a planar trajectory  $x_j(t)$ . In the plane, a stationary critical curve  $\mathcal{C}$  was found by Synge (1949) for parabolic cases. Each point on  $\mathcal{C}$  corresponds to a radial spatial trajectory either moving away or towards the origin with similar  $\Delta_p$  expanding  $\dot{p} > 0$ , or contracting  $\dot{p} < 0$ , respectively. The latter would lead to coalescence of three vortices. According to the spatial trajectories, the critical curve is partitioned into expanding or contracting branches. It was shown by Tavantzis and Ting (1988) that the expanding radial (spatial) trajectories are stable while the contracting ones are unstable. In this paper we show that a contracting radial trajectory slightly disturbed will depart from the radial line, move along a spatial trajectory nonsimilar to the initial configuration and eventually approach a radial expanding trajectory. Thus we come to the conclusion that three distinct vortices almost never coalescence.

## References

- [1] W. Gröbli, Specielle Probleme über die Bewegung geradliniger paralleler Wirbelfäden. Zürich: Zürich and Furrer, 1877.
- [2] J. Synge, On the motion of three vortices. *Can. J. Math.* 1949; 1; 257-270.
- [3] E. Novikov, Dynamics and statistics of a system of vortices. *Sov. Phys. JETP* 1975; 41; 937-943.
- [4] H. Aref, Motion of three vortices. *Phys. Fluids* 1979; 22; 393-400.
- [5] J. Tavantzis, L. Ting, The dynamics of three vortices revisited. *Phys. Fluids* 1988; 31; 1392-1409.
- [6] O. Knio, L. Collorec, D. Juvé, Numerical study of sound emissions by 2D regular and chaotic configurations. *J. Comput. Phys.* 1995; 116; 226-246.
- [7] D. Blackmore, L. Ting, O. Knio, “Studies of perturbed three vortex dynamics”, *J. Math. Phys.*, Vol. 48, 065402, pp. 1–30, 2007.
- [8] L. Ting, O. Knio, D. Blackmore, “Dynamics of Planar Vortex Clusters with Binaries” presented in Minisymposium IC/MP/107/R/520, 2nd part, “Recent Advances in Vortex Dynamics: Theory and Computation”, ICIAM-07, Zurich, July 16-20, 2007. To appear in the Proc. ICIAM-07.
- [9] Knio, D. Blackmore, L. Ting, “Numerical Study of Dynamics of Point Vortex Configurations”, presented at ICCES08, 17-22 March 2008, Hawaii.
- [10] C. C. Lin, “On the motion of vortices in two-dimensions”, Toronto Univ. Press, Toronto, 1943.

- [11] P. Newton, *The N-Vortex Problem*, Springer, New York, 2001.
  
- [12] L. Ting, D. Blackmore, Bifurcation of motions of three vortices and applications, presented in ICTAM-04, Session FM25, *Vortex Dynamics*, Warsaw, Poland, XXI ICTAM 2004 Abstracts and CD-ROM Proceedings, pp. 188-189.
  
- [13] H. Lamb, *Hydrodynamics*, 6th ed., Dover republ. New York, 1945.